Spectroscopic characterization, X-ray molecular structures and cyclic voltammetry study of two (piperazine) cobalt(II) meso-arylporphyin complexes. Application as a catalyst for the degradation of 4-nitrophenol

Mouhieddinne Guergueb, Soumaya Nasri, Jihed Brahmi, Youssef O. Al-Ghamdi, Frédérique Loiseau, Florian Molton, Thierry Roisnel, Vincent Guerineau, Habib Nasri

Spectroscopic characterization, X-ray molecular structures and cyclic voltammetry study of two (piperazine) cobalt(II) *meso*-arylporphyin complexes. Application as a catalyst for the degradation of 4-nitrophenol.

Mouhieddinne Guergueb [a], Soumaya Nasri[*a,b],Jihed Brahmi [a] , Youssef O. Al-Ghamdi [b], Frédérique Loiseau [c] , Florian Molton [c],Thierry Roisnel [d],Vincent Guerineau [e], Habib Nasri[*a]

[a]: University of Monastir, Laboratory of Physical Chemistry of Materials, Faculty of Sciences of Monastir, Avenue de l'environnement, 5019 Monastir, Tunisia.
[b]: Department of Chemistry, College of Science Al-Zulfi, Majmaah University, Saudi Arabia.
[c]: Département de Chimie Moléculaire, 301 rue de la Chimie, Université Grenoble Alpes, CS 40700, 38058 Grenoble Cedex 9, France.
[d]: Institute of Chemical Sciences of Rennes, UMR 6226, University of Rennes 1, Beaulieu Campus, 35042 Rennes, France.
[e]: Institut de Chimie des Substances Naturelles CNRS, Avenue de la Terrasse, F-91198, Gif-sur-Yvette, France

Abstract

Two new cobaltous-porphyrin complexes, namely (μ-piperazine)-bis[(*meso*-tetra(*para*-methoxyphenyl)porphyrinato)]cobalt(II) and (piperazine)[*meso*-tetra(*para*-chlorophenyl)porphyrin]cobalt(II) dichloromethane disolvate, with the formulas [{Co^{II}(TMPP)}$_2$(μ_2-pipz)] (complex **1**) and [Co^{II}(TClPP)(pipz)]·2CH_2Cl_2 (complex **2**), were used efficiently as catalysts in the degradation of 4-nitrophenol (4-NP) in an aqueous hydrogen peroxide solution. These cobalt(II)-pipz porphyrin complexes were characterized by a variety of spectroscopic methods including infrared, UV-visible, fluorescence, proton nuclear magnetic resonance, electron paramagnetic resonance (EPR) as well as mass spectrometry. A cyclic voltammetry investigation was also carried out on these two Co(II) metalloporphyrins. The EPR results indicate that both complexes **1** and **2** are paramagnetic low-spin (S = 1/2) cobalt(II) porphyrin complexes. Furthermore, the X-ray diffraction crystal structures of **1** and **2** were determined, and the intermolecular interactions were investigated by Hirshfeld surface analysis.

Corresponding author: Fax: + 966 0164044044
E-mail address: soumaya.n@mu.edu.sa (Soumaya Nasri)

Keywords: Cobalt(II) porphyrins, X-ray molecular structure; EPR spectroscopy; Photophysical properties; Degradation of 4-nitrophenol.

1. Introduction

Pollution is one of the biggest problems that threatens life on earth, as it continues to grow and gets worse over time. Water pollution is considered the most important among the other types of pollution, given the very serious consequences of water pollution on fauna and flora and to humans **[1,2]**. The chemical industries, producing pesticides and herbicides, release a number of nitrophenolic products into wastewater, including 4-nitrophenol (4-NP), also called p-nitrophenol or 4-hydroxynitrobenzene **[3,4]**. It is very toxic to human health where it can damage, for example, the nervous system and kidneys **[5,6]**. It is for these reasons that the US Environmental Protection Agency placed 4-NP on the list of the most dangerous and polluting chemicals **[7-9]**. Among the many methods used to remove 4-NP from wastewater are adsorption **[10]**, electrochemistry **[11,12]** and homogeneous and heterogeneous catalytic hydrogenation transfer **[13,14]**. It is noteworthy that many investigations concerning the degradation of 4-NP by cobalt species are reported in the literature **[15-17]**. These are concerned with the "cobalt ferrite core and graphitic shell ($CoFe_2O_4$/MGNC)" system using stoichiometric amounts of hydrogen peroxide for the degradation of an aqueous solution of 4-NP **[15]**. A water soluble cobalt phthalocyanine was also used for the degradation of 4-NP **[17]**. On the other hand, a number of papers have been published concerning the use of compounds involving cobalt as a catalyst in the reduction of 4-nitrophenol to 4-aminophenol **[18,19]**.

In addition to the methods mentioned above, a number of investigations concerning the treatment of wastewater containing hazardous organic products use porphyrin compounds as catalysts. These tetrapyrrole compounds are used alone but often they are combined with other species, such as metal salts, TiO_2, reducing agents such as $NaBH_4$ and oxidants such as H_2O_2. The use of these porphyrinic compounds lies in the fact that these species are very stable **[20-23]**. Indeed, porphyrins and metalloporphyrins are multifunctional π-electron conjugated macrocycles presenting optical and physical chemical properties that have exhibited great potential applications in catalysis **[24,25]**, electrochemical sensors **[26]**, antimicrobial materials **[27]**, photodynamic and photothermal therapy **[28,29]**, cell imaging **[30]** and several other applications. It should be noted that during the last few years, our research group has published a number of articles concerning the use of several porphyrin complexes in the catalytic degradation of some organic dyes **[31-33]**.

The first part of our work reported in this article concerns the synthesis of two piperazine cobalt(II) complexes with the *meso*-tetra(*para*-methoxyphenyl)porphyrin (H_2TMPP) and the *meso*-tetra(*para*-chlorophenyl)porphyrin (H_2TClPP). The formulas of these coordination compounds, as determined by single crystal X-ray molecular structures, are $[\{Co^{II}(TMPP)\}_2(\mu_2\text{-pipz})]\cdot 2CH_2Cl_2$ (pipz = piperazine) (**1**)

and [Co^{II}(TClPP)(pipz)]·2CH_2Cl_2 (**2**). These two cobaltous species were characterized by IR, UV-visible, fluorescence, ^{1}H NMR, EPR spectroscopy, ESI-mass spectrometry and cyclic voltammetry. In the second part of the present paper, we report the catalytic degradation of 4-nitrophenol (4-NP) using our two synthetic complexes.

2. Results and discussion

2-1. Synthesis of 1 and 2

The overall synthetic route for the preparation of *meso*-tetra(*para*-methoxyphenyl)porphyrin (H_2TMPP), *meso*-tetra(*para*-chlorophenyl)porphyrin (H_2TClPP), [Co^{II}(TMPP)] and [Co^{II}(TClPP)] starting material complexes, as well as the new cobaltous-pyrazine coordination compounds [{Co^{II}(TMPP)}$_2$(μ_2-pipz)]·2CH_2Cl_2 (pipz = piperazine) (**1**) and [Co^{II}(TClPP)(pipz)]·2CH_2Cl_2 (**2**), is depicted in Scheme 1 (see synthetic procedures in the supplementary information). These two formulas are attributed according to the X-ray molecular structures of these two species, but in organic solvents these two cobaltous metalloporphyrins are most likely to be of the pentacoordinated type [Co^{II}(Porph)(pipz)] (Porph = TMPP or TClPP) complexes.

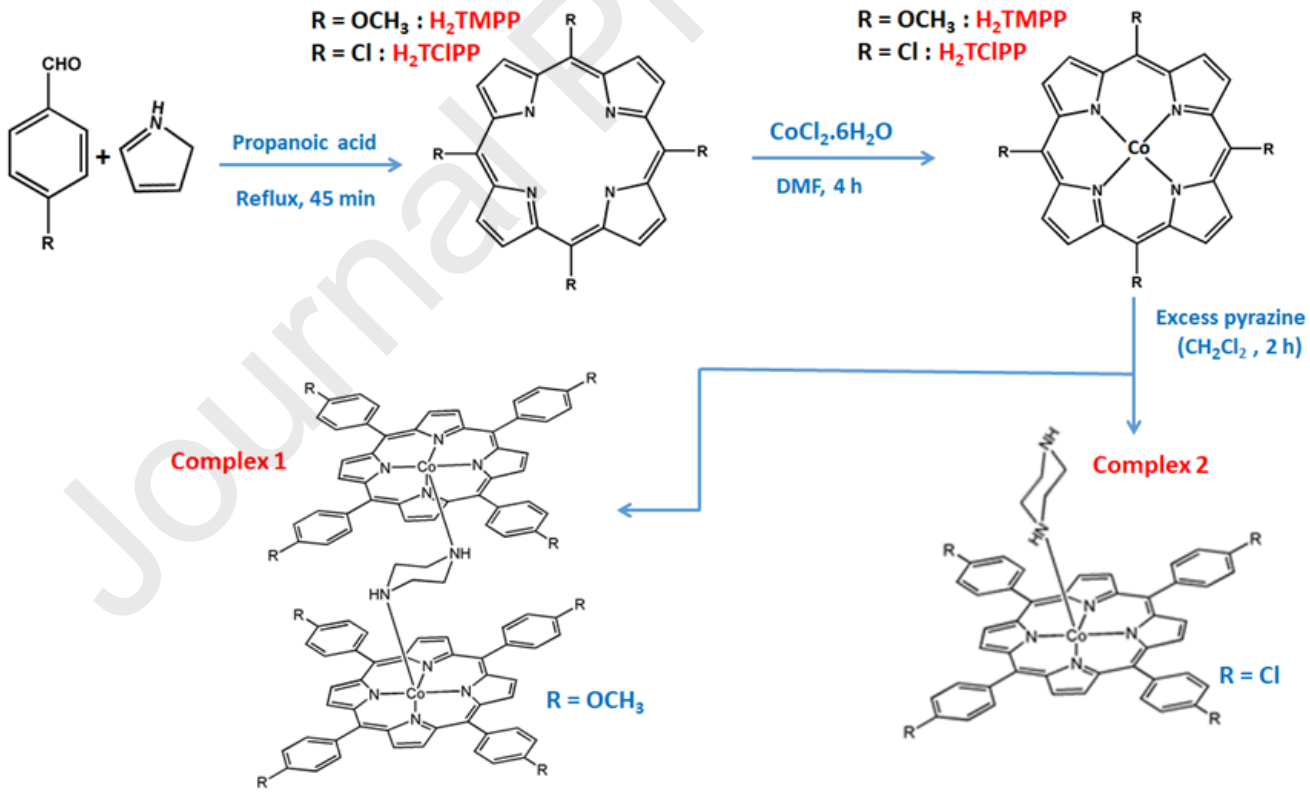

Scheme 1. Synthesis of the H_2TMPP and H_2TClPP free base porphyrins, the starting materials [Co^{II}(TMPP)] and [Co^{II}(TClPP)] and complexes **1** and **2**.

2.2. X-ray molecular structures of 1 and 2

Complexes **1** and **2** crystallize in the monoclinic and triclinic unit cells. The asymmetric unit of **1** contains a half [{Co^{II}(TMPP)}$_2$(μ_2-pipz)] dimer and one dichloromethane solvent molecule. For complex **2**, the asymmetric unit is made by a full [Co^{II}(TClPP)(pipz)] molecule and two disordered dichloromethane molecules, which were omitted by the SQUEEZE procedure **[34]**. In Tables S1 and S2 the structural refinement details and selected bond lengths and angles for complexes **1** and **2** are reported, respectively. The ORTEP diagrams of our two Co(II)-pipz coordination compounds are illustrated in Figures 1 and 2. For **1** and **2**, the Co(II) central metal is coordinated by the four N atoms of the pyrrole rings of the porphyrin ring and the N atom of the piperazine axial ligand. The coordination polyhedra of the Co(II) ions of the two piperazine derivatives **1** and **2** are illustrated in Figure S1. The Co–N(pipz) bond lengths of **1** and **2** are close, with values of 2.247(3) and 2.225(5) Å, respectively which are also close to that of the related species [Co^{II}(TPP)(pipz-S)] (pipz-S = piperazin-1-yl)sulfonyl)naphthalen-1-amine) with a Co–N(pipz) distance value of 2.241(5) Å **[35]**. We notice that the cobalt(II)-pipz non-porphyrinic complexes present Co–N(pipz) bond lengths in the range 2.196–2.2461(6) Å (Table 1), which are comparable with those of our Co(II)-pipz derivatives **1** and **2**. As shown by Figure S1, the piperazine axial ligand in both complexes **1** and **2** adopts the chair configuration, where the pipz molecule is nearly parallel to the porphyrin macrocycle for the dimer (**1**), while for the monomer species (**2**), the axial ligand molecule is nearly perpendicular to the porphyrin core. The C–C and C–N bond lengths of the pipz ligand for **1** and **2** are very close, while the C-C-C and C-N-C angles are smaller for the dimer complex **1**, which is most probably due to the constraint applied by the two [Co(TMPP)] moieties on the pipz ligand.

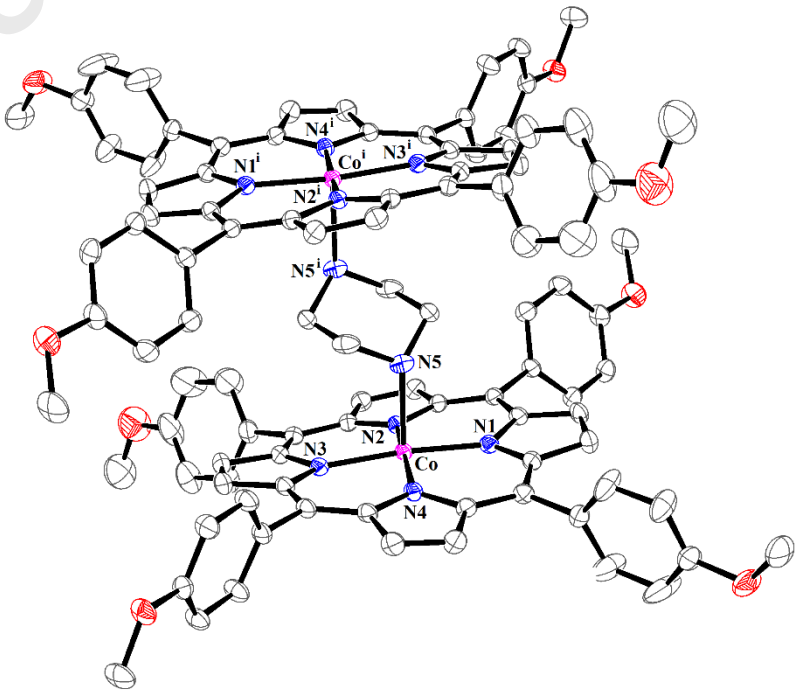

Figure 1. ORTEP diagram of [{Co^{II}(TMPP)}$_2$(μ_2–pipz)] (**1**). Ellipsoids are contoured at the 30% probability level and hydrogen atoms are omitted for clarity.

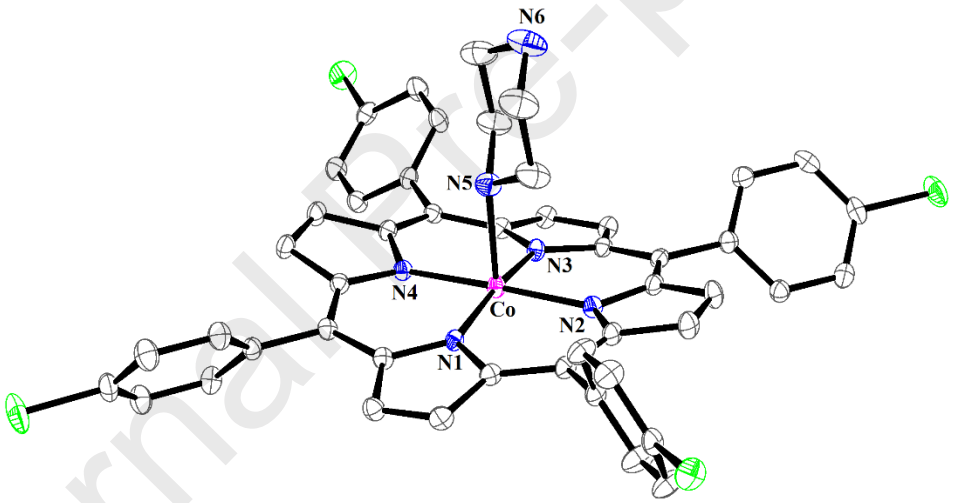

Figure 2. ORTEP diagram of [Co^{II}(TClPP)(pipz)] (**2**). Ellipsoids are contoured at the 30% probability level and hydrogen atoms are omitted for clarity.

It has been reported **[36]** that the mean equatorial distance between the cobalt ion and the four nitrogen atoms of the porphyrin core (Co–Np distance) is related to the *ruffling* distortion of the porphyrin core (Figure 9) where the Co–Np distance increases as the *ruffling* decreases. This type of deformation is described by high displacement values of the *meso*-carbons alternatively above and below the 24-atom mean plane of the porphyrin macrocycle. As shown in Table 1, the [Co(TPP)] **[37]** (TPP = *meso*-tetraphenylporphyrinato) complex exhibits the shortest Co–Np distance (1.923 Å), corresponding to the most important *ruffling* deformation of cobaltous *meso*-arylmetalloporphyrins. The displacements of each atom from the $C_{20}N_4$ mean plane (P_C) are shown in Figure 3. The Co–Np distance of complex **1** is 1.976(3) Å, which is higher than that of complex **2** with a value of 1.980(2) Å. This is in accordance with

the fact that the dimer species (**1**) exhibits higher *ruffling* than the monomer Co(II)-pipz derivative (**2**). Furthermore, the Co—Np values of **1** and **2** are close to those of related cobaltous pentacoordinated complexes of the type [Co^{II}(Porph)(L)] (Porph = *meso*-arylporphyrin, L = N-donor neutral ligand).

Table 1. Selected bond lengths [Å] and angles [°] for [{Co^{II}(TMPP)}$_2$(μ_2-pipz)].2CH_2Cl_2 (**1**) and [Co^{II}(TClPP)(pipz)] (**2**),

Complex	Porphyrin core[a] deformation type	M–N_p[b]	M–X_L[c]	M–P_C[d]	Ref.
	Piperazine cobalt(II) porphyrin complexes				
[Co^{II}(TPP)][e]	Ruf (+++)	1.923	-	0.050	**[37]**
[Co^{II}(TPP)(pip)$_2$][e,f]	Planar	1.987	2.436 (2)	0.000	**[38]**
[Co^{II}(TCPP)(py)$_2$][g]	Ruf(++)	1.961	1.958	0.000	**[39]**
[Co^{II}(TPP)(pipz-S)][i]	Sad(+), Ruf(+)	1.989 (5)	2.241 (5)	0.134	**[35]**
[{Co^{II}(TMPP)}$_2$(μ_2-pipz)] (**1**)	Ruf(+),sad (+++)	1.976 (3)	2.247 (3)	0.1298 (9)	this work
[Co^{II}(TClPP)(pipz)] (**2**)	Ruf (-),sad (++)	1.980 (2)	2.225 (2)	0.0885 (5)	this work
[Co^{II}(TMPP)(4-CNpy)]	Ruf(+),sad (+)	1.984 (3)	2.210 (3)	0.1404 (8)	**[33]**
[Co^{II}(TClPP)(4-CNpy)]	Ruf (+++),sad(+)	1.977 (2)	2.196 (3)	0.1440 (7)	**[33]**
	Piperazine zinc(II) porphyrin complexes				
[Zn^{II}(TPBP)(pipz)][j]	M-Sad, m-Dom	2.079 (2)	2.127 (2)	0.4365 (4)	**[58]**
	Piperazine-Co(II) non-porphyrinic complexes				
[Co^{II}(NCS)$_2$(MeOH)$_2$(pipz)$_2$]	-	-	2.196	-	**[40]**
[$Co^{II}Cl_2$(pipz)$_2$]	-	-	2.2461 (6) 2.2453 (6)	-	**[41]**
{[{$Co^{II}Cl_2$}(μ_2-(pipz)]}$_n$	-	-	2.070 (2) 2.051 (2)	-	**[42]**
[Co_2(bpdc)$_2$-(μ_2-prz)(H_2O)$_2$][j]	-	-	2.135(2)	-	**[43]**

[a]: See the description of the different types of the porphyrin core deformation in the text, *Planar* designates a planar porphyrin core. "+": moderate, "++": important, "+++": very important and "-": weak deformation. [b]: M–N_p = average equatorial distance between the center metal and the nitrogen atoms of the pyrroles, [c]: M–X_L = Distance between the metal atom and the coordinated atoms of the axial ligands, [d]: M–P_C = Distance between the metal atom and the mean plane made by the 24-atom core of the porphyrin (P_C). [e]: TPP = *meso*-tetraphenylporphyrinato, [f]: pip = piperidine, [g]: TCPP = *meso*-tetra(4-carboxyphenyl)porphyrinato,[i]: pipz-S= piperazin-1-yl)sulfonyl)naphthalen-1-amine,[j]: TPBP = *meso*-[tetrakis-[4-(benzoyloxy)phenyl]porphyrinate, [j]: H_2bpdc = 2,20-bipyridine-6,6'-dicarboxylic acid.

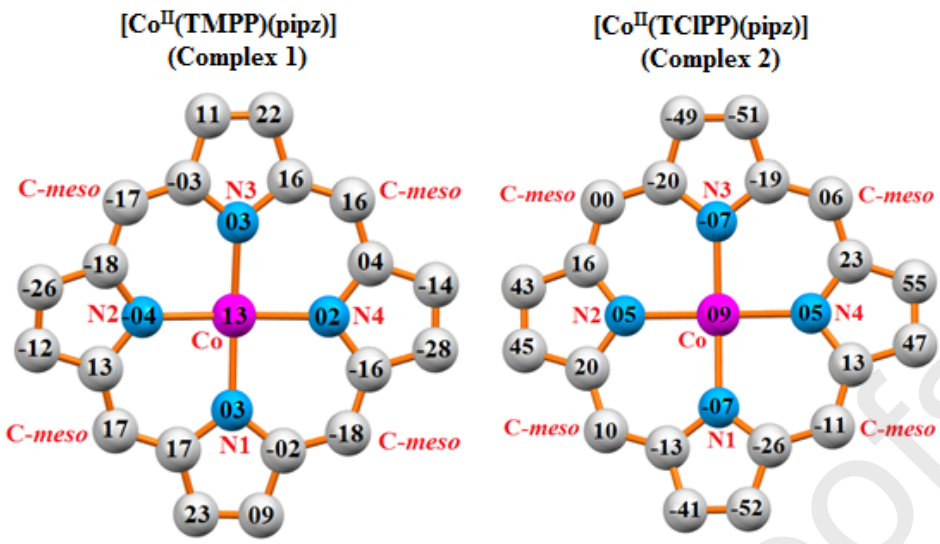

Figure 3. Formal diagrams of the porphyrinato cores of **1** (left) and **2** (right).

As indicated in Figure 4, complex **1** presents a long Co···Co distance with a value of 8.867 Å. However, this is not the case for complex **2** for which the Co···Co value is very short (5.225 Å) and the value of the distance between two adjacent average planar porphyrin (P_C) rings of the 24 atoms is 4.264 Å, We can explain the formation of " dimers" between the [Co^{II}(TClPP)(pipz)] molecules in the case of the crystal lattice of the TClPP porphyrinate and not in the case of the TMPP moiety by the bulky disordered OMe group in the *para* position of the phenyls of the *meso*-arylporphyrin compared to the chlorine atoms placed at the same *para*-phenyl position of the TClPP derivative, which are less sterically hindering groups.

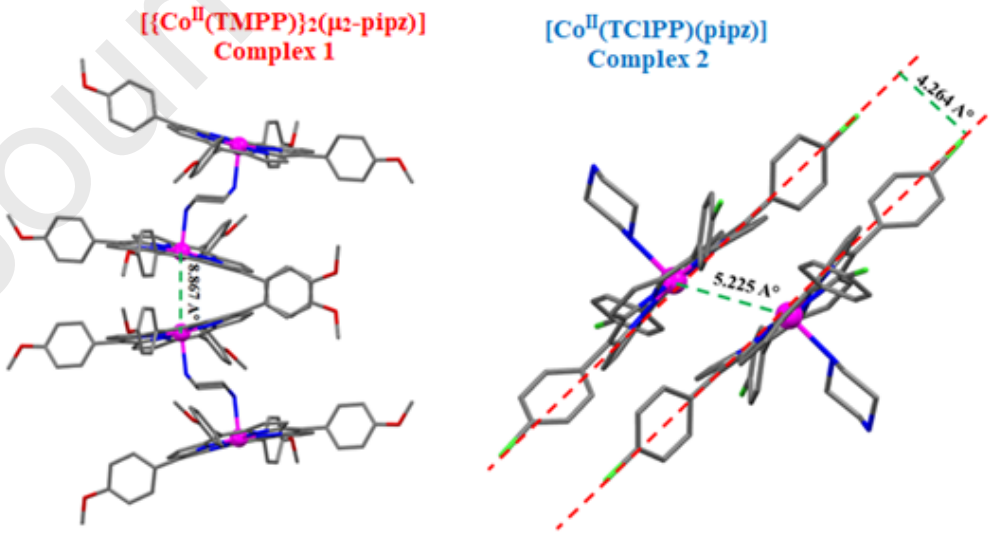

Figure 4. Drawing showing the Co···Co interaction for complexes **1** and **2**.

2.3. Hirshfeld surface analysis

In order to get a better insight into the intermolecular interactions of **1** and **2**, Hirshfeld surfaces **[44]** incorporating two-dimensional (2D) fingerprint plots **[45]** were determined using the CrystalExplorer **[46]** program. Hirshfeld surfaces are used (1) to visualize the intermolecular interactions using colors, (2) to represent short and long contacts and (3) to indicate the relative strength of interactions.
The "d_{norm}" function, given by the equation below, represents the ratio involving the distances from all surface points to the nearest internal "d_i" and external "d_e" atoms and the van der Waals radii:

$$d_{norm} = \frac{di - rivdW}{rivdW} + \frac{de - revdW}{revdW}$$

where «d_e» is the distance from the point to the nearest nucleus external to the surface, «d_i» is the distance to the nearest nucleus internal to the surface and « vdW » is the van der Waals radii of the atom **[46]**. The d_{norm} surface is mapped on the Hirshfeld surface with red, white and blue colors. The d_{norm} value is zero (white color) when the intermolecular contacts are equal to the van der Waals radii, the d_{norm} value is negative (red) when the intermolecular contacts are shorter than the van der Waals radii and positive (blue) when they are longer. Furthermore, a red concave area of the Hirshfeld surface is shown around an acceptor atom and a blue concave region is located around a donor atom. The 2D fingerprint plots (d_i versus d_e) present contacts between two atom interactions and indicate the percentage of contributions from different interaction types **[47]**. Surface plots for d_{norm} (Figures 5-a and S2) are generated using a high standard surface resolution over a color scale of -0.19 to 1.6 Å for complex **1** and -0.14 to 3.4 Å for complex **2**. The distribution of fingerprint patterns on the Hirshfeld surfaces for structures **1** and **2** are illustrated in Figure 5-d. For **1**, the intermolecular H···H contributions are 46.2 % with approximately minimum distance of (d_e+d_i) around 2.6 Å, where the proportion of H···C/C···H, H···Cl/Cl···H and H···O/O···H are 23.2% (d_e + d_i=2.85 Å), 11% (d_e+d_i =3.1 Å) and 10.7% (d_e + d_i=2.7 Å), respectively. In the case of complex **2**, the intermolecular H···H contributions are 35.6 % with approximately minimum distance of (d_e+d_i) around 2.4 Å, where the proportion of H···Cl/Cl···H, H···C/C···H and H···N/N···H are 31.6% (d_e+d_i = 3 Å), 21.2% (d_e+d_i =2.8 Å) and 4.3% (d_e+d_i = 2.6 Å), respectively (FigureS3). In Figure 11 the relative percentage contributions of the other intermolecular contacts that contribute to the Hirshfeld surfaces in **1** and **2** are represented. The curvedness and shape index are also used to indicate the packing modes and how neighboring molecules are linked together. The shape index for **1** and **2** exhibits a red concave region on the surface near the acceptor atom and a blue region around the donor atom (Figure 5-b). The curvedness is defined as a function of the root mean square curvature of the surface.

The curvedness maps for **1** and **2** present no flat surface patches, indicating the absence of stacking. Schematic illustrations of the decomposed fingerprint plots into the different contacts within complexes **1** and **2** are shown in Figure 6.

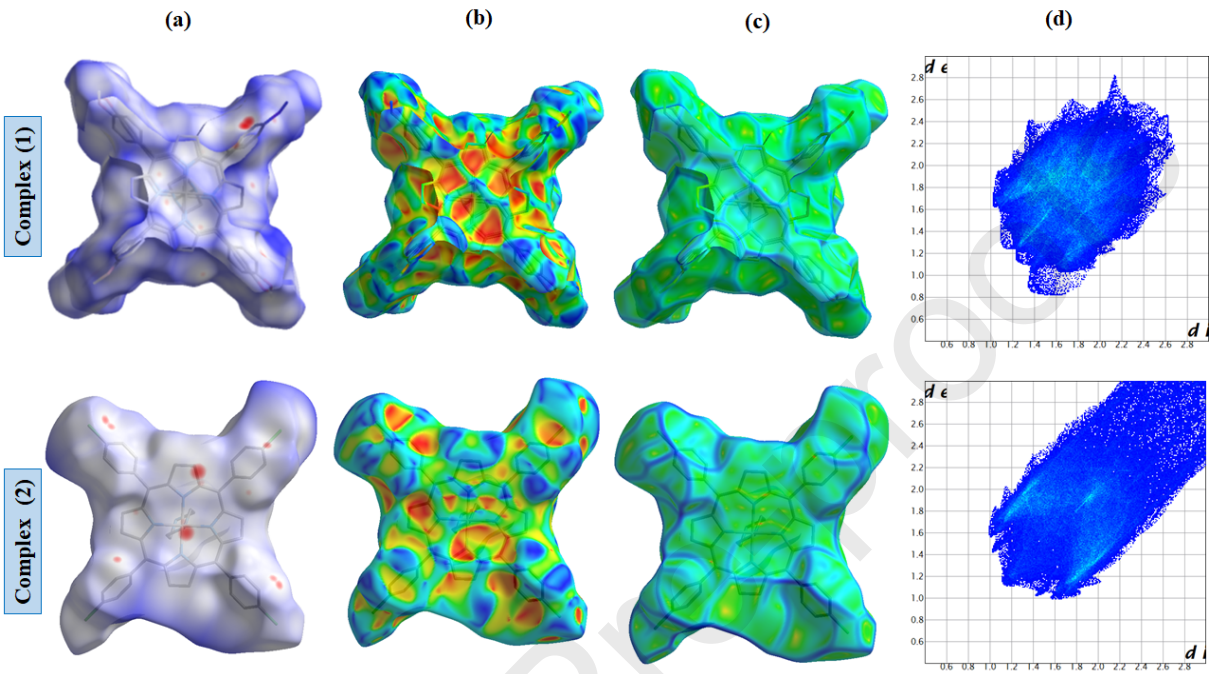

Figure 5. **(a):** Hirshfeld surfaces mapped with d_{norm} ranging from -0.19 (red) to 1.6 Å (blue) for complex **1** and -0.14 (red) to 3.4 Å (blue) for complex **2**, **(b):** the shape index, **(c):** the curvedness and **(d):** 2D fingerprint plots with d_i and ranging from 0.6 to 2.8 Å for **1** and **2**.

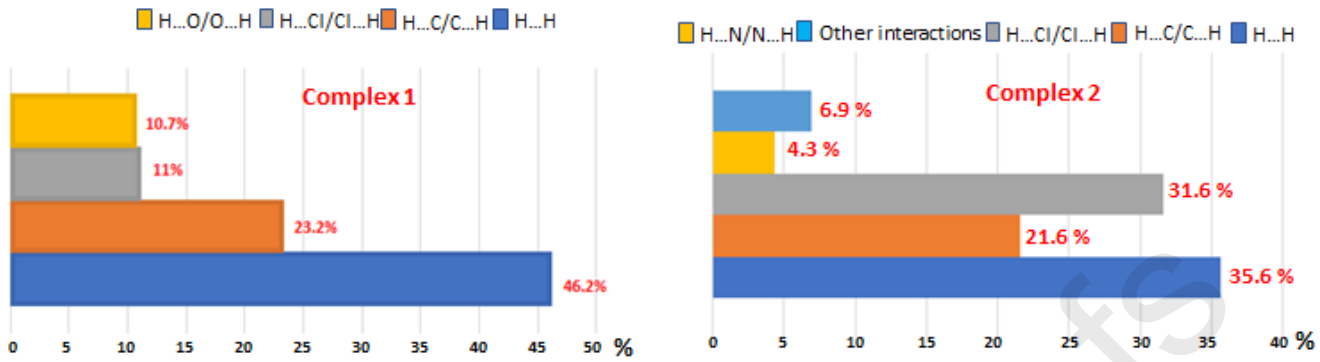

Figure 6. Schematic illustration of the decomposed fingerprint plots into the different contacts within complexes **1** and **2**.

2-4. IR and ^{1}H NMR spectroscopy

The IR data of **1** and **2** are characteristic of *meso*-arylporphyrin coordination compounds, with absorption bands attributed to the ν(CCH) and δ(CHC) vibrations in the range 2960-2840 cm^{-1} and at ~ 1000 cm^{-1}, respectively. Organic compounds containing an N–H group, such as piperazine (pipz), present N–H stretching absorption bands in the 3500-3200 cm^{-1} region **[48]**. The wavenumber value of the absorption band corresponding to ν(NH) for the non-coordinated pipz molecule is 3250 cm^{-1} and this is shifted to 3368 and 3279 cm^{-1} when coordinated to the cobalt ion in complexes **1** and **2** respectively.

^{1}H NMR is an important spectroscopic method to differentiate between a diamagnetic cobalt(III) *meso*-arylporphyrin complex with the $3d^6$ ground state electronic configuration and a paramagnetic cobaltous *meso*-arylporphyrin species with the $3d^7$ ground state electronic configuration **[49]**.

Mansour *et al.,* **[49]** reported that cobalt(III) *meso*-aryporphyrin derivatives exhibit β-pyrrolic and phenyl ring protons ($H_{o,o'}$, $H_{m,m'}$ and H_p) slightly shifted compared to those of the corresponding free base porphyrins, with chemical shift values of about δ 8.5 and 9 ppm for the β-pyrrolic protons and between δ 8.5 and 7.5 ppm for the phenyl protons (Table 2). The β-pyrrolic (Hβ) and the phenyl proton peaks for Co(II) *meso*-arylmetalloporphyrins are downfield shifted with chemical shift values between δ 12 and 16.5 ppm for the Hβ protons and between δ 14 and 8 ppm for the H-phenyl protons (Table 2). The ^{1}H NMR spectra of our Co(II)-pipz porphyrin species (**1** and **2**) are illustrated in Figures S4 and S5, while the NMR data are reported in Table 2 for these species, the free bases porphyrins H_2TMPP, H_2TClPP, the [Co^{II}(TMPP)] and [Co^{II}(TClPP)] starting materials and a selection of related porphyrinic compounds. The

NMR results of **1** and **2** indicate clearly that these derivatives in $CDCl_3$ solution are paramagnetic cobaltous porphyrinic complexes. The coordination of the piperazine ligand to the central metal for complexes **1** and **2** is confirmed by the signals of the -CH_2- and the NH protons of the pipz ligand at δ 4.15 / 1.65 and 3.78 / 1.35 ppm, respectively.

Table 2. ^{1}H NMR data for our porphyrinc species and for the selected free base *meso*-arylporphyrins and cobalt *meso*-arylporphyrin complexes (spectra recorded in $CDCl_3$).

Compound	Hβ-pyrrolic protons	H-phenyl protons	H-OCH_3[a]	Ref.
Meso-arylporphyrins				
H_2TPP[b]	8.84	8.23; 7.91; 7.67; 7.26	-	**[49]**
H_2TpivPP[c]	8.82	8.70; 7.88; 7.50	-	**[49]**
H_2TMPP	8.86	8.08; 7.27;	4.10	this work
H_2TClPP	8.89	8.18; 7.74 -	-	this work
Co(III)-meso-arylporphyrins				
$[Co^{III}(TPP)Cl(DMI)]$[b,d]	8.83	7.87; 7.65	-	**[50]**
$[Co^{III}(TPP)(DMI)]^+$[b,d]	8.95	7.86; 7,71	-	**[50]**
$[Co^{III}(TPP)Cl(py)]$[b]	9.00	8.80; 7.70	-	**[50]**
$[Co^{III}(TPP)(N_3)(py)]$[b]	9.22	8.38; 7.80	-	**[51]**
Co(II)-meso-arylporphyrins				
$[Co^{II}(TMPP)]$	15.90	13.10; 9.43	5.25	this work
$[Co^{II}(TClPP)]$	15.75	12.93; 9.9 -	-	this work
$[Co^{II}(TPP)]$[b]	15.75	13.10; 9.80; 7.95	-	**[49]**
$[Co^{II}(TpivPP)]$[c]	15.30	11.50; 10.90; 7.80	-	**[49]**
$[Co^{II}(TPP)(HIm)]$[b,e]	12.8	8.8; 8,40; 7.69	-	**[52]**
$[Co^{II}(TPP)(py)]$[b]	12.50	8.5; 8.33; 7.82	-	**[52]**
$[\{Co^{II}(TMPP)\}_2(\mu_2\text{-pipz})]$ (**1**)	15.89	13.15;9.51	5.42	this work
$[Co^{II}(TClPP)(pipz)]$ (**2**)	13.39	9.89; 8.85	-	this work
$[Co^{II}(TMPP)(4\text{-CNpy})]$.	14.64	11.42: 8.87; 9.01	5.01	**[33]**
$[Co^{II}(TClPP)(4\text{-CNpy})]$	14.61	11.53; 9.01; 9.42	-	**[33]**

[a]: H-OCH_3= protons of the OCH_3 group in the *para*-phenyl positions of the H_2TMPP porphyrin, [b]: TPP = *meso*-tetraphenylporphyrinato, [c]: TpivPP = *meso*-[α,α,α,α-tetrakis(*o*-pivalamidophenyl)]porphyrinato, [d]: DMI = N,N'-dimethylimidazolylidene, [e]: HIm = imidazole.

2.5. Photophysical properties of 1 and 2

The tetracoordinated cobaltous metalloporphyrins of the type $[Co^{II}(Porph)]$ (Porph = *meso*-arylporphyrin) exhibit λ_{max} Soret band values at ~410 nm in organic solvents. The addition of N-donor aromatic neutral ligands to these porphyrinic Co(II) derivatives leads to a redshift of the Soret and Q(0,0) bands with λ_{max} values at ~435 and ~555 nm, respectively. The corresponding species are in the majority of cases pentacoordinated Co(II) complexes of the type $[Co^{II}(Porph)(L)]$ (L = N-donor neutral ligand) or

hexacoordinated coordination compounds of the type [Co^{II}(Porph)$(L)_2$]. In our case, complexes **1** and **2** present Soret bands at 438 and 336 nm, respectively and Q bands at 556; 597 and 553; 592 nm, respectively (Figure 7, Table 3). These values are very close to those of related pentacoordinated and hexacoordinated cobalt(II) *meso*-aryporphyrin metalloporphyrins (Table 3). This confirms the [Co^{II}(TClPP)(pipz)] formula of complex **2** in the solid state, as determined by its X-ray molecular structure. For complex **1**, which is a dimer in the solid state with the formula [{Co^{II}(TMPP)}$_2$(μ_2-pipz)], the UV-visible spectroscopy shows that in solution, this species can be either a monomeric or dimeric pentacoordinated cobalt(II) complex. This result is confirmed by a mass spectrometry study. On the other hand, our cobaltous [Co^{II}(TMPP)] and [Co^{II}(TClPP)] complexes and complexes **1** and **2** present optical gap values (Eg-opt) of ~ 2.00 eV, determined using the Tauc plot method (Figure 8).

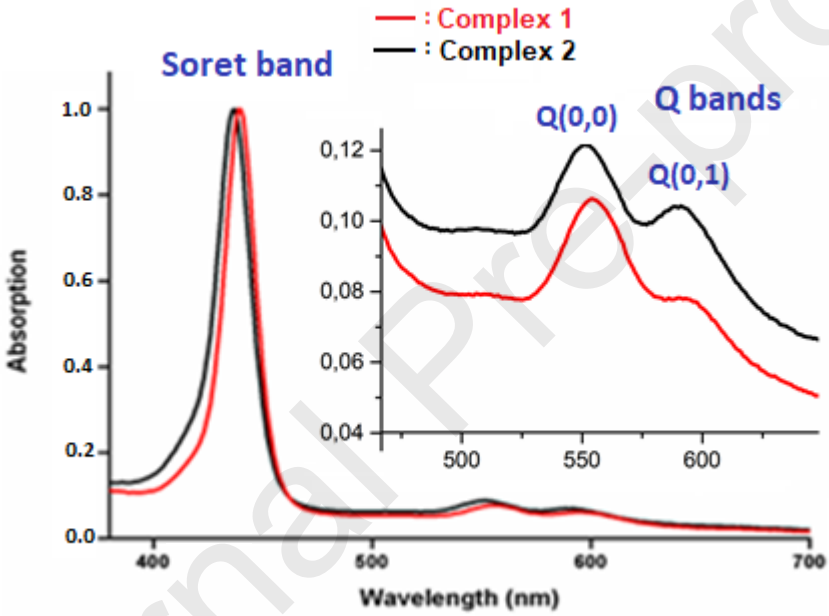

Figure 7. Electronic absorption spectra of **1** and **2** at ca.10^{-6} M in dichloromethane. The inset shows an enlarged view.

Table 3. UV-visible data of **1** and **2** and a selection of *meso*-arylporphyrins and Co(II) metalloporphyrin coordination compounds. The spectra were recorded in dichloromethane.

Complex	Soret band	Q bands		$E_{gap-opt}$ (eV)	Ref.
	λ_{max} (nm) (ε x 10^{-3})				
	Cobaltous meso-arylporphyrin complexes				
[Co^{II}(TPP)][a]	412	528	-	-	**[49]**
[Co^{II}(TpivPP)][b]	412	524	-	-	**[49]**
[Co^{II}(TPBP)][c]	412	528		-	**[54]**

[Co^{II}(TClPP)]	412(380)	529(64)-	2.01	this work
[Co^{II}(TMPP)]	414(450)	535(23)	2.11	this work
[Co^{II}(TPBP)(4,4'-bpy)$_2$][c,d]	435(562)	552(30)		**[53]**
[Co^{II}(TPP)(Hon)$_2$][b,e]	434	555 -		**[54]**
[Co^{II}(TMPP)(4-CNpy)]	437(420)	558(40)600(35)	2.003	**[33]**
[Co^{II}(TClPP)(4-CNpy)]	436(453)	556(49)598(44)	1.971	**[33]**
[{Co^{II}(TMPP)$_2$(μ_2-pipz)] (**1**)	438(401)	556(47) 597(36)	1.960	this work
[Co^{II}(TClPP)(pipz)] (**2**)	436(399)	553(43) 592(31)	2.000	this work

[a]: TPP = *meso*-tetraphenylporphyrinato, [b]: TpivPP = α,α,α,αtetrakis(*o*-pivalamidophenyl)porphyrinato, [c]: TPBP = *meso*-[tetrakis-[4-(benzoyloxy)phenyl]porphyrinato, [d]: 4,4'-bpy = 4,4'-bipyridine, [g]: Hon = 2-aminophenol.

The emission spectra of porphyrins and metalloporphyrins exhibit two transition types. The first, which is the strongest, is the $S_1 \rightarrow S_0$ transition, concerning the Q bands, and it is between the first excited singlet state S_1 to the ground state S_0. The second emission transition type is the $S_2 \rightarrow S_0$ transition; the Soret band is from the second excited singlet state S_2 to the ground state S_0. This second transition is so weak that it is usually neglected compared to the $S_1 \rightarrow S_o$ transition. The emission spectra of complexes **1** and **2** in dichloromethane and ethanol (concentrations ~ 10^{-6} M) are depicted in Figure 8 and the λ_{max} value of the emission Q bands, the fluorescent lifetime (τ_f) values and the fluorescence quantum yield (Φ_f) values are given in Table 4, as well as the corresponding data for several related cobaltous porphyrin species. Figure S9 illustrates the fluorescence decays for **1** and **2**.

Table 4. Emission data for complexes **1** and **2** and some related cobaltous metalloporphyrins.

Complex	Temp. (K)	Solvent	λ_{max} (nm)		Φ_f	τ_f (ns)	Ref.
			Q(0,0)	Q(0,1)			
[{Co^{II}(TMPP)}$_2$(μ_2-pipz)](**1**)	298	CH_2Cl_2	653	719	0.026	1.57	this work
	77	Ethanol	648	710	-	6.10	
[Co^{II}(TClPP)(pipz)] (**2**)	298	CH_2Cl_2	651	717	0.042	1.51	this work
	77	Ethanol	640	711	-	5.90	
[Co^{II}(TPBP)(4,4'-bipy)$_2$][a]	298	CH_2Cl_2	652	718	0.036	-	**[53]**
[Co^{II}(TMPP)(4-CNpy)]	298	CH_2Cl_2	652	717	0.054	1.970	**[33]**
[Co^{II}(TClPP)(4-CNpy)]	298	CH_2Cl_2	653	714	0.060	1.997	**[33]**

[a]: TPBP = *meso*-[tetrakis-[4-(benzoyloxy)phenyl]porphyrinato.

The λ_{max} values of the Q(0,0) and Q(0,1) emission bands of **1** and **2** (in dichloromethane at 298 K and in ethanol at 77 K) are 653 / 648 and 719 / 710, and 651 / 640 and 717 / 711 nm, respectively. These values are very close to those of other related cobaltous pentacoordinated porphyrins (Table 4). The fluorescence quantum yields (Φ_f) values of **1** and **2** dichloromethane at 298 K are 0.026 and 0.042, respectively. These later two values are close to those of the related Co(II) porphyrins given in Table 4.

The single photon counting technique was used to measure the lifetime of singlet excited state (τ_f), while the fluorescence decays were fitted to single exponentials. Complexes **1** and **2** exhibit lifetime values (τ_f) of ~6.0 ns in ethanol solution at 77 K, while in dichloromethane solution and at room temperature, the τ_f values of **1** and **2** are ~1.5. The Φ_f and τ_f values shown by cobaltous metalloporphyrins could be explained by the paramagnetic nature of the cobalt(II) metal anion which allows inter system crossing to the triple state and therefore lowering the fluorescence **[55]**.

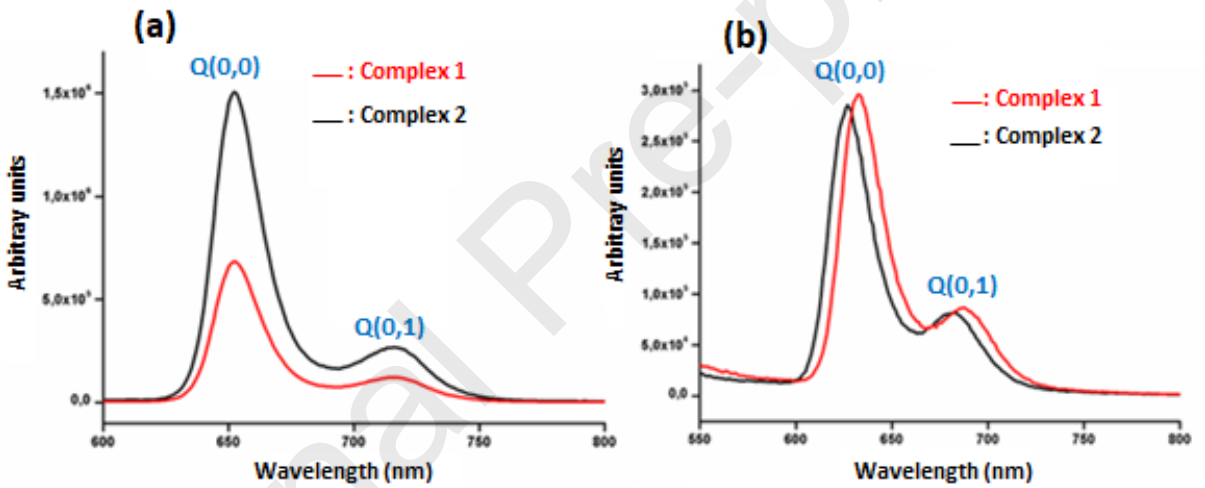

Figure 8. Emission spectra of **1** and **2**. **(a):** Spectra recorded at room temperature in dichloromethane, **(b):** spectra recorded at 77 K in ethanol (concentrations ~ 10^{-6} M).

2.6. Cyclic voltammetry investigation

The cyclic voltammograms (CV) of complexes **1** and **2** recorded in dichloromethane are depicted in Figures 9 and 10 and the electrochemical data of these two Co(II) piperazine complexes are given in Table 5, along with those of several reported porphyrin derivatives. We recently reported a detailed description of the CV investigations on cobaltous metalloporphyrins in non-chlorinated solvents, such as THF and DMSO, and in dichloromethane solvent **[33]**. The CV data of our Co(II)-pipz derivatives are similar to those of the tetracoordinated [Co^{II}(Porph)] (Porph = TMPP or TClPP) starting materials and the

pentacoordinated [Co^{II}(Porph)(4,4'-bipy)] complexes (4,4'-bipy = 4,4'-bipyridine) (Table 5). The first one-electron reduction wave of **1** and **2** is attributed to the Co(II)/Co(I) center ion reduction (**RM1,OM1**) with half potential values of ~ -0.82 V. The first one-electron ring reduction (**R4,O4**) presents $E_{1/2}$ values of -1.39 and -1.30 V for **1** and **2**, respectively. The first irreversible oxidation wave of **1** and **2** is assigned to the Co(II)/Co(III) oxidation (**MO2,MR2**) with E_{ap}(anodic potential) values of 0.21 and 0.56 V for **1** and **2**, respectively. For complex **1** the first (**O1,R1**), the second (**O2,R2**) and the third (**O3,R3**) waves are irreversible, with E_{ap} values of 1.20, 1.51 and 1.99 V, respectively. In the case of complex **2**, these three one electron ring oxidation waves are reversible, with $E_{1/2}$ values of 1.35, 1.56 and 1.90 V, respectively.

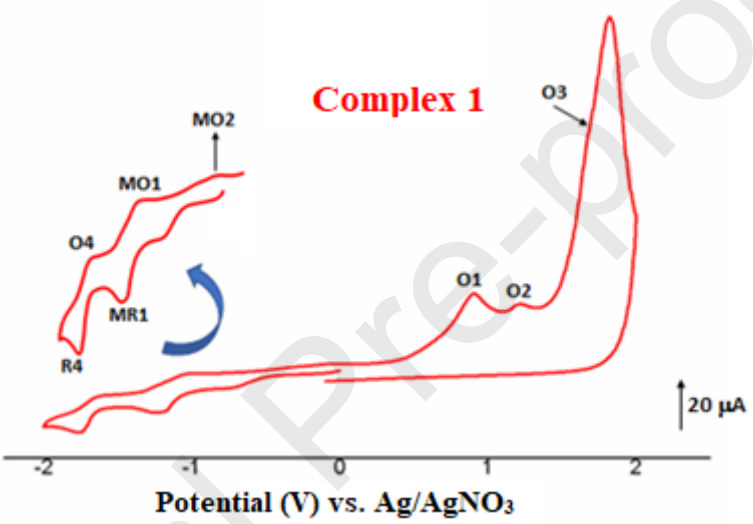

Figure 9. Cyclic voltammogram of **1**. The solvent is dichloromethane, and the concentration is ca. 10^{-3} M in 0.2 MTBAP, 100 mV s^{-1}, vitreous carbon working electrode (Ø = 2 mm). The inset shows the enlarged view.

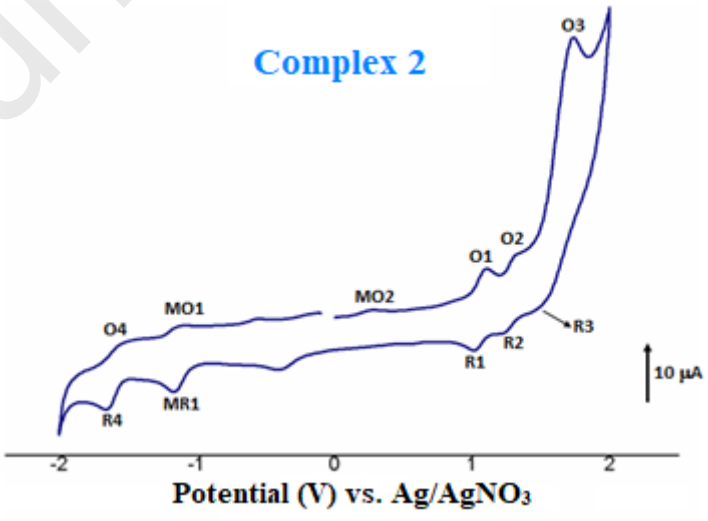

Figure 10. Cyclic voltammogram of **2**. The solvent is dichloromethane, and the concentration is ca. 10^{-3} M in 0.2 MTBAP, 100 mV s^{-1}, vitreous carbon working electrode (Ø = 2 mm).

An inspection of Table 5 shows that (i) except the case of the [Co^{II}(TMPP)(4,4'-bipy)] complex **[33]** where the $E_{1/2}$ value of the first ring oxidation wave (**O1,R1**) is smaller than that of the starting material [Co^{II}(TMPP)], the other pentacoordinated cobaltous complexes exhibit potential values ($E_{1/2}$ and E_{ap}) shifted to more positive values than those of the [Co^{II}(Porph)] corresponding species, (ii) it seems that the oxidation potentials are independent of the nature of the *meso*-arylporphyrin and also of the nature of the axial ligand and (iii) the $E_{1/2}$ values of the Co(II)/Co(I) reduction and especially the values of $E_{1/2}$ of the central Co(II)/Co(III) ion of the cobaltous metalloporphyrins, including **1** and **2**, are shifted to more negative values with respect to the [Co^{II}(Porph)] starting materials. It should be noted that the large shift towards negative potentials of the Co(II)/Co(III) oxidation waves compared to the shift in Co(II)/Co(I) reduction is an indication that the Co(III) porphyrin complexes are much more stable than those of the cobaltous metalloporphrins **[56]**.

In conclusion, the CV study shows that the donor or acceptor nature of the phenyl *para* groups of TMPP and TClPP porphyrinato ligands and the nature of the axial N-donor ligand do not have much effect on the electrochemical properties of complexes **1** and **2**.

Table 5. Electrochemical data [a]for H_2TMPP, H_2TClPP, complexes **1** and **2** and a selection of *meso*-porphyrins and Co(II) *meso*-metalloporphyrins. All the data are obtained from voltammograms recorded in dichloromethane.

	Oxidations				**Reductions**			Ref.
	1st Porph Oxid (O1,R1)	2nd Porph Oxid (O2,R2)	3rd Porph Oxid (O3,R3)	Oxid. Co(II)/Co(III) (MO2)	1st Porph Red (R4,O4)	2nd Porph Red (R3,O3)	Red Co(II)/Co(I) (MR1,MO1)	
	$E_{1/2}$[b]	$E_{1/2}$	$E_{1/2}$	$E_{1/2}$	$E_{1/2}$	$E_{1/2}$	$E_{1/2}$	
Free bases meso- arylporphyrins								
H_2TMPP	1.02	1.19	1.67*	-	-1.19	-1.52	-	this work
H_2TClPP	1.00	1.23	1.53	-	-1.09	-1.41	-	this work
H_2TPP[c]	1.02	1.26	-	-	-1.20	-1.55	-	**[57]**
H_2TPBP[d]	0.95	1.36	1.48	-	-1.12	-1.53	-	**[58]**
Tetracoordinated cobalt(II) metalloporphyrins								
[Co^{II}(TClPP)]	1.00	1.26	1.85	0.60*	-1.40	-	-0.88	this work
[Co^{II}(TMPP)]	0.93	1.20	-	0.70*	-1.36	-	-0.70	this work
[Co^{II}(TPP)][c]	1.16	-	-	0.98	-1.40*	-	-0.83	**[59]**
[Co^{II}(TPP)][c]	0.97	-	-	0.78	-	-	-0.85	**[60]**
[Co^{II}(TPP)][c]	0.91	-	-	0.75	-	-	-	**[61]**
Pentacoordinated cobalt(II) metalloporphyrins								
[[Co^{II}(TMPP)}$_2$(μ_2-pipz)] (**1**)	1.20*	1.51*	1.99*	0.21	-1.39	-	-0.82	this work
[Co^{II}(TClPP)(pipz)) (**2**)	1.35	1.56	1.90	0.56	-1.30	-	-0.83	this work
[Co^{II}(TMPP)(4-CNpy)]	0.89	1.25	1.78	0.47	-1.43	-	-0.94	**[33]**
[Co^{II}(TClPP)(4-CNpy)]	1.13	1.31	-	0.42	-1.32	-	-0.92	**[33]**
[Co^{II}(TPP)(py)][c]	-	-	-	-0.12	-	-	-1.16	**[59]**

*: irreversible wave, [a]: The potentials are reported versus SCE, [b]: $E_{1/2}$ = half wave potential, [c]: TPP = *meso*-tetraphenylporphyrinato, [d]:TPBP = *meso*-[tetrakis-[4-(benzoyloxy)phenyl]porphyrinate.

2.7. Electron Paramagnetic Resonance (EPR) investigation of complexes 1 and 2

The first EPR published investigations on cobalt(II) porphyrin complexes date back to the sixties and early seventies, especially that by Assour *et al.,* in 1965 **[62]**, Walker *et al.,* in 1970 **[63]** and Wayland *et al.*, in 1974 **[64]**. All these early investigations show that cobaltous metalloporphyrins present a single unpaired electron in the d_{z^2} orbital. In fact, these heme-like cobaltous derivatives are low-spin (S = 1/2) where the ground state of the electronic configuration of the Co(II) ion is $\left[(d_{xy})^2(d_{yz})^2(d_{yz})^2(d_{z^2})^1\right]$ **[62]**. It has been reported that pentacoordinated cobaltous porphyrins of the type [Co^{II}(Porph)(L)] (Porph = *meso*-arylporphyrin and L = amine-type axial ligand) exhibit axial symmetric EPR spectra with g// (g parallel) and $g_\perp$ (g perpendicular) values of 2.03 and 2.32 respectively **[65]**. For these species, the in-plane Co(II) hyperfine tensor ($A_\perp$) cannot be resolved, whereas typically $A_{//}$ = 8 mT and each of the eight nuclear sublevels (cobalt nucleus I = 7/2) carries a discernible super hyperfine coupling due to the N-donor axial ligand (e.g. ^{14}N).

The solid X-band EPR spectra of **1** and **2** recorded at 7 K are depicted in Figure 11. The EPR parameters of these species, along with several other related cobaltous metalloporphyrins, are given in Table 6. A close investigation of Table 6 indicates that the pentacoordinate [Co^{II}(Porph)(L)] complexes present $g_\perp$ and $g_{//}$ values of ~3.30 and ~2.02, respectively which are quite a bit higher than those of the [Co^{II}(Porph)] starting materials, tetracoordinated derivatives with $g_\perp$ and $g_{//}$ values of ~2.25 and ~1.78, respectively. The EPR spectrum of our Co(II)-TMPP-pipz derivative (**1**) is of the axial type with a $g_\perp$ ($g_x = g_y = g_\perp$) value of 2.301 and a $g_{//}$ (g_z) value of 1.995 at 7 K. At 100 K, the $g_\perp$and g// values of 1 are practically the same as those at 7 K. The Co(II)-TClPP-pipz species (**2**) presents a rhombic type X-band solid EPR spectrum with g_x, g_y and g_z values at 7 K of 2.350, 2.301 and 1.996, respectively. The rhombic character of the EPR spectrum of **2** is confirmed by the Q-band EPR spectrum (Figure 12) of this coordination compound, which clearly shows the three well separated bands corresponding to g_x, g_y and g_z. The g values of **1** are very close to those of complex **2** at 100 K. We noticed that the $g_\perp$ value of **1** is close to the g_x and g_y values of **2** and g// of **1** is also very close to g_z of complex **2**. These values, which are similar to those of the reported pentacoordinate low-spin cobaltous porphyrins with an N-donor neutral axial ligand, such as pyridine and imidazole (Table 6), indicate that complexes **1** and **2** are also low-spin (S = 1/2). Furthermore, the X-band EPR spectra of **1** and **2** at 7 K were successfully fitted with S = 1/2 (Figures S10 and S11).

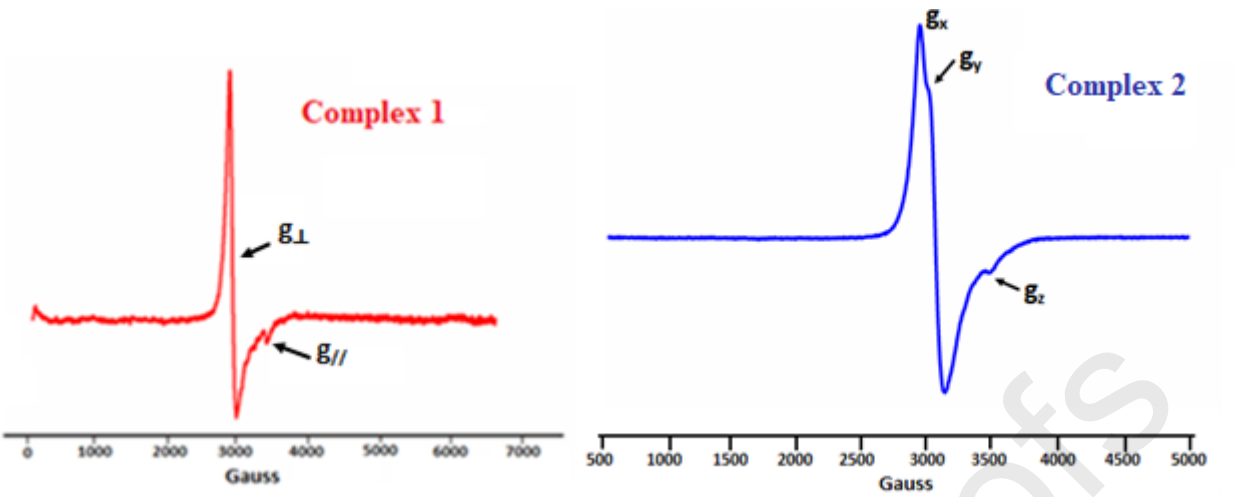

Figure 11. The X-band EPR spectra for **1** and **2** (powder) at 7 K (perpendicular polarization). EPR conditions: microwave frequencies of 9.6418 and 9.6417 GHz for **1** and **2** respectively, microwave power of 6.5 mW

Table 6. EPR data for complexes **1** and **2** and a selection of low-spin cobalt(II) metalloporphyrins.

Complex		T (K)	$g_{\perp}(g_x, g_y)$	$g_{//}$ (g_z)	Ref.
Tetracoordinated Co(II) porphyrin complexes					
[Co^{II}(TMPP)]	powder	77	3.285	1.790	**[63]**
[Co^{II}(TPP)]	powder	77	3.222	1.798	**[62]**
Pentacoordinated Co(II) porphyrin complexes					
[Co^{II}(TMPP)(py)]	in toluene	77	2.327	2.025	**[64]**
[Co^{II}(TPP)(py)]	in toluene	77	2.320	2.028	**[65]**
[Co^{II}(TMPP)(pip)]	in toluene	77	2.318	2.026	**[63]**
[Co^{II}(TPP)(HIm)]	in toluene	77	2.318	2.030	**[65]**
[{Co^{II}(TMPP)}$_2$(μ_2-pipz)] (**1**)	powder	100 7	2.337 2.301	1.994 1.995	this work
[Co^{II}(TClPP)(pipz)] (**2**)	powder	100 7	2.350; 2.305 2.350; 2.301	1.990 1.996	this work

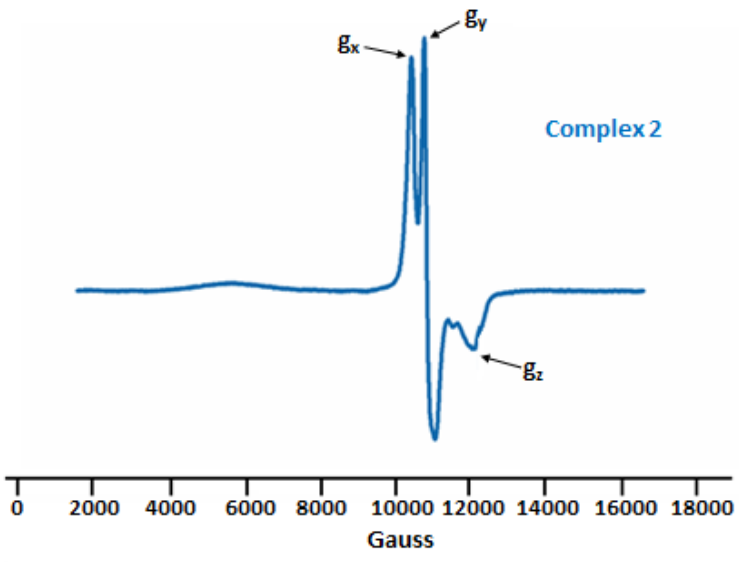

Figure 12. The Q-band EPR spectrum for **2** (powder) at 7 K (perpendicular polarization). EPR conditions: microwave frequency of 33.9292 GHz, microwave power of 6.5 mW

The most important results of this EPR investigation are: (i) both complexes **1** and **2** are cobaltous low-spin (S = 1/2) metalloporphyrin species, (ii) the nature of the *meso*-arylporphyrin and the N-donor axial (such as py, Him, pipz) of the cobaltous pentacoordinated porphyrin complex have little effect on the EPR parameters of these species and (iii) for these Co(II) low-spin porphyrin coordination compounds, there is no clear relationship between the EPR parameters (e.g., g values and spectrum shape, for example) and the molecular structures of these complexes (monomer or dimer, space group type, etc.).

2.8. Kinetic adsorption of the 4-NP compound using complexes 1 and 2

Adsorption can be defined as the interaction between a chemical species (adsorbate) from a gas, liquid or solid to a surface (adsorbent). The adsorption process is due to weak physicochemical forces, such as hydrogen bonds **[66]** and van der Waals forces **[67]**. Figure S12 shows the absorbance of 4-NP in aqueous solution in the presence of complexes **1** and **2** with different adsorption times. In our case, the adsorption of the 4-NP molecule on the cobaltous [Co^{II}(Porph)(pipz)] complexes **1** and **2** is probably due to π-π stacking between the TMPP and TClPP porphyrin macrocycles and the phenyl ring of the 4-NP adsorbate rather than coordination of the dye molecule with the central metal Co(II) ion which is already coordinated to a pipz molecule, given that cobaltous metalloporphyrins are usually pentacoordinate.

The decrease of the π-π* electron transition band at 400 nm of 4-NP as a function of time in the presence of **1** and **2** indicates a concentration decrease of this species, consistent with the adsorption of 4-NP on complexes **1** and **2**.The adsorbent capacity (q_t) and the decolorization yields (***R%***) are given by the following relationships, **Eq. 1** and **Eq. 2**, respectively:

$$q_t\,(\mathrm{mg.g^{-1}}) = (C_o - C_t).(V/m) \qquad \textbf{Eq. 1}$$

where C_o and C_t are the dye concentration at the instant $t = 0$ and t. V represents the volume of 4-NP used and m is the mass of the adsorbent.

$$R\% = (A_o - A_t)/A_o.100 \qquad \text{Eq. 2}$$

where A_o and A_t are the absorption at $t = 0$ and at the t instant.

The decolorization yields (***R%***) and the adsorption capacities (q_t) of the 4-NP compound in the presence of complexes **1** and **2** as a function of time are represented in Figure 13. The ***R%*** values for the complexes **1** and **2** are 25.9, and 30.8 %, respectively.

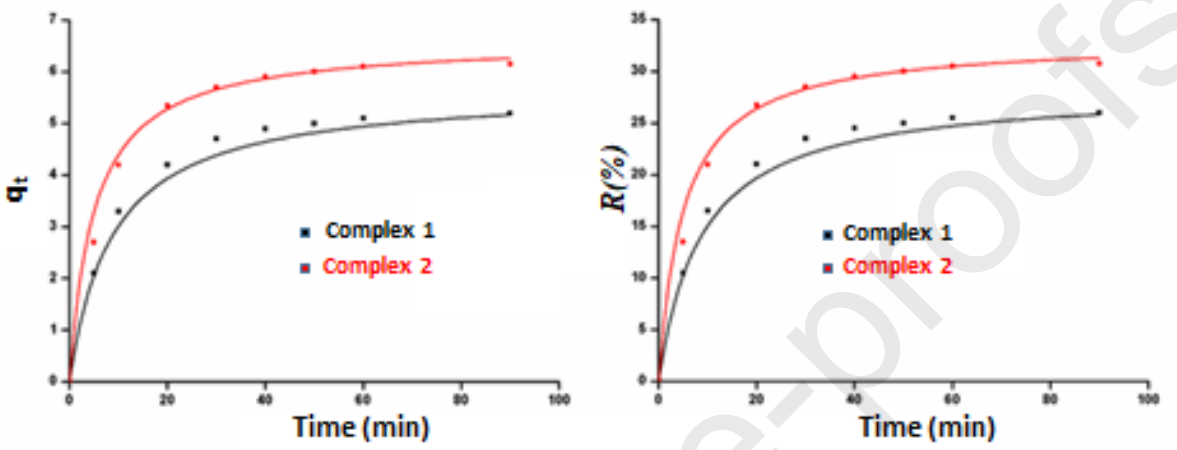

Figure 13. **(a):**Adsorption capacity (q_t) and **(b):** Adsorption efficiency (***R%***) curves of 4-NP as a function of time with the porphyrin compounds **1** and **2**. C_0 = 20 mg/l, m = 5 mg, pH =8.

We used four theoretical kinetic approaches to understand the adsorption process between the 4-NP organic species and our two cobaltous derivatives **1** and **2,** which are: the pseudo first order, the pseudo second order, the Elovich and the intra-particular Diffusion models **[68]**. The plots corresponding to these four kinetic models are illustrated in Figure S13. The regression coefficient R^2 values were used to evaluate the kinetic results obtained using these four models and the results are given in Table 7. Thus, the pseudo second order model gives the better fit for both complexes **1** and **2**. This result is consolidated by the fact that the experimental q_t value is very close to the theoretical q_t value obtained using the pseudo second order model (Table 7).

Table 7. Kinetic data for the adsorption of 4-NP on complexes **1** and **2**.

Calculated parameters	**1**	**2**
q_{exp} (mg g^{-1})	5.25	6.35
Pseudo first Order		
k_1 (min^{-1})	0.05	0.04

q(mg g^{-1})	3.43	3.16
R^2	0.97	0.86
Pseudo second order		
k_2 (g mg^{-1} min^{-1})	0.02	0.03
q_{cal} (mg g^{-1})	5.67	6.61
R^2	0.99	0.99
Elovich		
α (mg g^{-1} min^{-1})	2.05	3.54
β (mg g^{-1} min^{-1})	0.91	0.84
R^2	0.94	0.90
Intra-particulardiffusion		
K_d (mg g^{-1} $min^{-1/2}$)	0.55	0.64
C (mg g^{-1})	1.02	1.42
R^2	0.85	0.82

k_1 = the pseudo first order rate constant (min^{-1}), k_2 = the pseudo second order rate constant (g mg^{-1} min^{-1}), α (mg g^{-1} min^{-1}) = the initial adsorption rate, β (g mg^{-1}): the desorption constant related to the extent of surface coverage and activation energy for chemisorption, k_d = the intra-particle diffusion rate constant (g mg^{-1} $min^{-1/2}$), *C (mg g^{-1})* = the thickness of the limited diffusion layer.

2.9. Degradation of the 4-NP compound using complexes 1 and 2

The ability of complexes **1** and **2** to catalyze the degradation of 4-NP was tested using an aqueous H_2O_2 solution at room temperature. The optimal condition for this degradation was found to be as follows: mass of **1** and **2** is m = 5 mg (0.0025 and 0.0055 mmol, respectively), the hydrogen peroxide aqueous solution is Co = 10 mg L^{-1} and pH = 8. Figure 14 represents the absorption of 4-NP in the absence of H_2O_2 (reference = blank experiment)and in the presence of a 20 mg L^{-1}(0.72 mmol) of an aqueous solution of 4-NP for several degradation times.

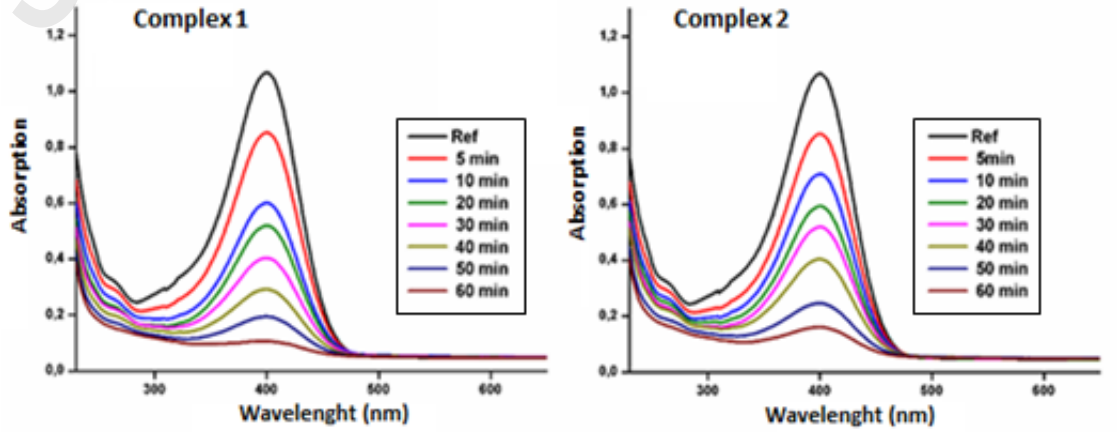

Figure 14. Variation of the λ_{max} values of the absorption bands of 4-NP in an aqueous hydrogen peroxide solution (10 mg L^{-1}) in the presence of complex **1** (left) and **2** (right).

The oxidation of organic compounds by hydrogen peroxide catalyzed by metallic species is known to involve the radical OH•, leading to the formation of intermediate species **[69]**. In our current case, the degradation rate of 4-NP can be obtained using the following equation (**Eq. 3**):

$$\frac{dC}{dt} = -k.C.[OH^{\cdot}] \quad \textbf{Eq. 3}$$

where C is the concentration of 4-nitrophenol at time t and k is defined as the second order rate constant of the 4-nitrophenol reacting with OH•. Given the fact that the concentration of OH• is constant, assuming the steady state situation for the formation rate of these intermediates **[70],** the equation can further be simplified. Therefore, the degradation rate of 4-NP due to the combination of H_2O_2 is given by the following equation (**Eq. 4**):

$$\frac{dC}{dt} = -k_o.C \qquad \textbf{Eq. 4}$$

Figure 15-a illustrates the C_t/C_o curves verses time. C_t and C_o are the concentration of 4-NP at the instants t and $t = 0$, respectively. The degradation yield ($R\%$) is given by the relation below (**Eq. 5**):

$$R(\%) = \left(1 - \frac{C_t}{C_o}\right).100. \qquad \textbf{Eq.5}$$

As shown by the same Figure 15-a, when we use only the 4-NP with the H_2O_2 solution, no degradation of the organic species occurs. When 4-NP and complex **1** (or **2**) were mixed, as shown by this figure,25.8 and 30.8 % of 4-NP were removed using complexes **1** and **2**, respectively. The use of an aqueous solution of H_2O_2 (C_o = 10 mg L^{-1}) leads to degradation yields of 97 and 95% for **1** and **2**, respectively, after 60 min of reaction. The k_o values of the pseudo-first order rate constant of the degradation concerning the "4-NP-H_2O_2 solution-complex **1** (or **2**)" systems are 5.96 × 10^{-2} min^{-1} (R^2 = 0.9982) and 4.88 × 10^{-2} min^{-1} (R^2= 0.9945), respectively. As mentioned in the introduction, a very

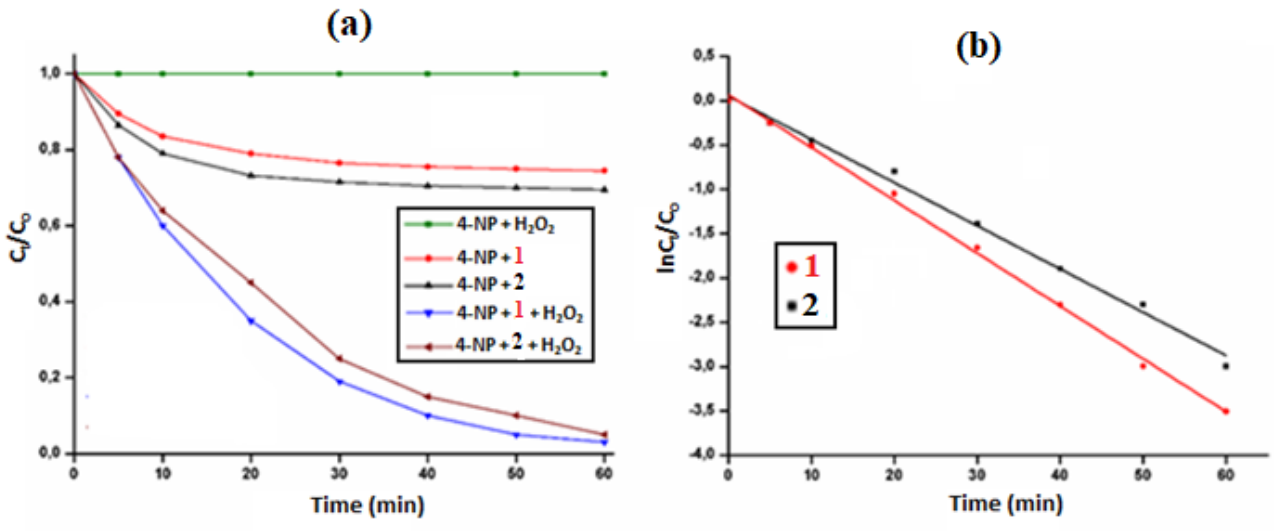

important number of investigations have been reported in the literature during the last decade concerning the degradation of the 4-nitrophenol **[71,76]**.

Figure 15. **(a):** Variation of C_t/C_o as a function of time. **(b):** Fitting data of the first-order pseudo kinetic curves for the « (4-NP)-(H_2O_2)-(complex **1** or **2**) » systems. Reaction conditions: $[4\text{-NP}]_o$ = 20 mg L^{-1}, $[H_2O_2]_o$ = 10 mg L^{-1}, pH = 8.

Table 8 summarizes the degradation yield and the reaction time of several methods used in the degradation of 4-NP.

Table 8. Selection of several methods used for 4-NP degradation with the optimal reaction conditions and yields.

Method of degradation	**Degradation system and optimal reacting conditions**	**Degradation yield, time reaction**	**Ref.**
Photodegradation in the presence of H_2O_2	UV-visible /aqueous H_2O_2, anion scavengers (HCO_3^-, NO_3^- and Cl^-), λ = 401nm, pH = 5,14, $[H_2O_2]_o$ = 0.50 mM,$[4\text{-NP}]_o$ = 50 ppm, room temperature	98% (12 min)	**[74]**
Catalyze: PVA/AgNPs nanocomposite film	Silver nanoparticles (AgNPs) doped Polyvinyl Alcohol (PVA) film	93% (25 min)	**[72]**
Photocatalytic degradation	TiO_2 nanoparticles incorporated with $CuInS_2$ clusters, 300W high pressure Hg lamp (l = 365 nm), $[4\text{-NP}]_o$ = 20 mh/L, m (catalysis) 25 mg, pH = 4.	99% (2 h)	**[75]**
Porphyrin-TiO_2 photocatalysts	TiO_2-CuPorph, 125 W, 24 V Iodine-Tungsten lamp, λ = 400 nm,	99.1% (400 mn)	**[76]**
Chemical catalysis	Complex **1** or **2** / H_2O_2 solution, $[4\text{-NP}]_o$ = 20 mg L^{-1}, $[H_2O_2]_o$ = 10 mg L^{-1}, pH = 8, room temperature.	93% (60 min)	this work

The chemical degradation using our cobaltous complexes **1** and **2** in hydrogen peroxide solution leads to an acceptable yield of 93% comparable to that using a system made by a PVA/AgNPs nanocomposite film as a catalyst **[71]**. We noticed that the photocatalytic degradation using TiO_2 systems presents high 4-NP yield degradation yields (Table 8). Notably, tetracoordinated metalloporphyrins of the type [M(Porph)] (M = central metal and Porph = *meso*-arylporphyrin) are usually used in a photodegradation of the 4-NP species where the metal cations are usually Cu(II), Zn(II), Pd(II), Fe(II) and Sn(IV) **[21,22,77]**. The only known example of a cobaltous metalloporphyrin in a 4-NP-TiO_2 photodegradation system is the $[Co^{II}(CPp)]$ complex where CPp is the *meso*-di[4-(carboethoxymethyleneoxy)phenyl]-10,20-di(4-butylphenyl)porphyrinate **[23]**.

3. Conclusion

We have prepared two piperazine cobaltous coordination compounds with the *meso*-tetra(*para*-methoxyphenyl)porphyrin (H_2TMPP) and the *meso*-tetra(*para*-chlorophenyl)porphyrin (H_2TClPP). The single crystal X-ray molecular structures of these two complexes show that the first species is a dimer with the formula $[\{Co^{II}(TMPP)\}_2(\mu_2\text{-pipz})]\cdot 2CH_2Cl_2$ (**1**) and the second derivative is pentacoordinated with the formula $[Co^{II}(TClPP)(pipz)]$ (**2**). Complexes **1** and **2** were characterized by UV-visible, fluorescence, IR, ^{1}H NMR, mass spectrometry and cyclic voltammetry and an EPR investigation indicated that both **1** and **2** are low-spin (S = 1/2) cobalt(II) porphyrin complexes. A degradation study of 4-nitropyridine (4-NP) dye using our two Co(II)-Porph-pipz derivatives (**1** and **2**) was carried out an aqueous hydrogen peroxide solution. which showed that the degradation yields are 97 and 95% for **1** and **2**, respectively after 60 min of reaction. Furthermore, the reduction efficiency values of 4-NP using complexes **1** and **2** are quite high, with values of ~94% for both species. Notably, complexes **1** and **2** have very similar spectral and electrochemical properties, which is also the case for the degradation of 4-NP where these compounds were used as catalysts and behaved in a very similar way.

Supporting information

Supplementary data associated with this article can be found in the online version. Complete crystallographic data for the structural analysis have been deposited with the Cambridge Crystallographic Data Centre; CCDC reference numbers 2023647 and 2023648. These data can be obtained free of charge via www.ccdc.cam.ac.uk/conts/retrieving.html (or from the Cambridge Crystallographic Data Centre, 12 Union Road, Cambridge CB2 1EZ, UK; fax: (+44) 1223 336033;
e-mail: deposit@ccdc.cam.uk).

Notes

The authors declare no competing financial interest.

Acknowledgements

The authors gratefully acknowledge financial support from the Ministry of Higher Education and Scientific Research of Tunisia. The authors extend their appreciation to the deanship of Scientific Research at Majmaah

University, Saudi Arabia. We also thank the IR-RPE CNRS FR3443 network for EPR analysis (Grenoble France).

References

[1] G. Salehi, R. Abazari, A. R. Mahjoub, *Inorg. Chem.*, 2018, 57, 8681–8691. https://doi.org/10.1021/acs.inorgchem.8b01636

[2] J. C. G. Sousa, A. R. Ribeiro, M. O. Barbosa, M. F. R. Pereira, A. M. T. Silva, *J. Hazard. Mater.,* 2018, 344, 146–162.https://doi.org/10.1016/j.jhazmat.2017.09.058

[3] Y. Qin, H. Zhang, Z. Tong, Z. Song, N. Chen, *J. Environ. Chem. Eng.*, 2017, 5, 2207–2213. https://doi.org/10.1016/j.compositesb.2020.108345

[4] W. Zhang, G. Li, W. Wang, Y. Qin, T. An, X. Xiao, W. Choi, *Appl. Catal. B*, 2018, 232, 11–18. https://doi.org/10.1016/j.apcatb.2018.03.006

[5] A. Kumar, A. Kumar, G. Sharma, A. H. Al-Muhtaseb, M. Naushad, A. A. Ghfar, C. Guo, F. J. Stadler, *Chem. Eng. J. (Lausanne)*, 2018, 339, 393–410. https://doi.org/10.1016/j.cej.2018.01.105

[6] C. Yin, J. Cai, L. Gao, J. Yin, J. Zhou, *J. Hazard. Mater.*, 2016, 305, 15–20. https://doi.org/10.1016/j.jhazmat.2015.11.028

[7] M. A. Callahan, Water-soluble environmental fate of 129 priority pollutants (Vol.1). Office of water planning and standards, Office of Water and waste management, US Environmental Protection Agency, (1979).

[8] Y. Ding, W. Bai, J. Sun, Y. Wu, M. A. Memon, C. Wang, C. Liu, Y. Huang, J. Geng, *ACS Appl. Mater. Interfaces*, 2016, 8, 12165–12175. https://doi.org/10.1021/acsami.6b02164.

[9] K. S. Shin, J.-Y. Choi, C. S. Park, H. J. Jang, K. Kim, *Catal. Lett.*, 2009, 133, 1. https://doi.org/10.1007/s10562-009-0124-7.

[10] E. Marais, T. Nyokong, *J. Hazard. Mater.*, 2008, 152, 293–301. https://doi.org/10.1016/j.jhazmat.2007.06.096.

[11] P. Cañizares, C. Sáez, J. Lobato, M. A. Rodrigo, *Ind. Eng. Chem. Res.*, 2004, 43, 1944–1951. https://doi.org/10.1021/ie034025t.

[12] F. D. Popp, H. P. Schultz, *Chem. Rev.,* 1962, 62, 19–40. https://doi.org/10.1021/cr60215a002.

[13] G. Brieger, T.J. Nestrick, *Chem. Rev.*, 1985, 85, 129-170. https://doi.org/10.1021/cr60291a003.

[14] Y. Yulizar, G. T. M. Kadja, M. Safaat, *React. Kinet. Mech. Catal.*, 2016, 117, 353–363. https://doi.org/10.1007/s11144-015-0916-2.

[15] R. S. Ribeiro, J. Gallo, M. Bañobre-López, A. M. T. Silva, J. Faria, H. T. Gomes, *Chem. Eng. J.,* 2019, 376, 120012, https://doi.org/10.1016/j.cej.2018.09.173.

[16] L. A. Frolova1,O. V. Khmelenko,*Catal. Lett*., 2021, 151, 1522-1533, https://doi.org/10.1007/s10562-020-03419-1.

[17] E. Tugba, S. K. Tekintas, *J. Mol. Struct.,* 2020, 1215, 128189, https://doi.org/10.1039/C6TA01054G,

[18] X. Li, C. Zeng, J. Jiang, L. Ai, *J. Mater. Chem. A*, 2016, 4, 7476-7482, https://doi.org/10.1039/C6TA01054G

[19] A. Mondal, A. Mondal, B. Adhikary, D. K. Mukherjee, *Bull. Mater. Sci*., 2017, 40, 321–328. https://doi.org/10.1007/s12034-017-1367-3.

[20] M. Rabbani, M. Heidari-Golafzani, R. Rahimi, *Mater. Chem. Phys.*, 2016, 179, 35–41. https://doi.org/10.1016/j.matchemphys.2016.05.005.

[21] M. Duan, J. Li, M. Li, Z. Zhang, C. Wang, *Appl. Surf. Sci.*, 2012, 258, 5499–5504.
[22] G. M. Mamardashvili, D. A. Lazovskiy, O. V. Maltceva, N. Zh. Mamardashvili, O. I. Koifman, *Inorg. Chim. Acta*, 2019, 486, 468–475.
https://doi.org/10.1016/j.apsusc.2012.02.069.
[23] X. Zhao, X. Liu, M. Yu, C. Wang, J. Li, *Dyes, Pigm.*, 2017, 136, 648–656.
https://doi.org/10.1016/j.dyepig.2016.09.025.
[24] K. S. Lokesh, A. Shambhulinga, N. Manjunatha, M. Imadadulla, M. Hojamberdiev, *Dyes Pigm.*, 2015, 120, 155–160.
https://doi.org/10.1016/j.dyepig.2015.04.002.
[25] P. Mineo, A. Abbadessa, A. Mazzaglia, A. Gulino, V. Villari, N. Micali, S. Millesi, C. Satriano, E. Scamporrino, *Dyes Pigm.*, 2017, 141, 225–234.
https://doi.org/10.1016/j.dyepig.2017.02.018.
[26] B. Kaur, K. Malecka, D. A. Cristaldi, C. S. Chay, I. Mames, H. Radecka, J. Radecki, E. Stulz, *Chem. Commun.*, 2018, 54, 11108–11111.
https://doi.org/10.1039/C8CC05362F.
[27] O. Lyutakov, O. Hejna, A. Solovyev, Y. Kalachyova, V. Svorcik, *RSC Adv.*, 2014, 4, 50624–50630.
https://doi.org/10.1039/C4RA08385G.
[28] M. E. Alea-Reyes, J. Soriano, I. Mora-Espí, M. Rodrigues, D. A. Russell, L. Barrios, L. Pérez-García, *Colloid Surf. B*, 2017, 158, 602–609.
https://doi.org/10.1016/j.colsurfb.2017.07.033.
[29] J. Zeng, W. Yang, D. Shi, X. Li, H. Zhang, M. Chen, *ACS Biomater. Sci. Eng.*, 2018, 4, 963–972.
https://doi.org/10.1021/acsbiomaterials.7b00886.
[30] N. C. M. Tam, P. Z. McVeigh, T. D. MacDonald, A. Farhadi, B. C. Wilson, G. Zheng, *Bioconjugate Chem.*, 2012, 23, 1726–1730.
https://doi.org/10.1021/bc300214z.
[31] R. Soury, M. Jabli, T. A. Saleh, W. Sattar Abdul-Hassan, E. Saint-Aman, F. Loiseau, C. Philouze, H. Nasri, *RSC Adv.*, 2018, 8, 20143–20156.
https://doi.org/10.1039/C8RA01134F.
[32] M. Guergueb, J. Brahmi, S. Nasri, F. Loiseau, K. Aouadi, V. Guerineau, S. Najmudin, H. Nasri, *RSC Adv.*, 2020, 10, 22712–22725.
https://doi.org/10.1039/D0RA03070H.
[33] M. Guergueb, S. Nasri, J. Brahmi, F. Loiseau, F. Molton, T. Roisnel, V. Guerineau, I. Turowska-Tyrk, K. Aouadi, H. Nasri, *RSC Adv.*, 2020, 10, 6900–6918.
https://doi.org/10.1039/C9RA08504A.
[34] A. L. Spek, *Acta Cryst C*, 2015, 71, 9–18.
https://doi.org/10.1107/S2053229614024929.
[35] J. Kim, S.-H. Lim, Y. Yoon, T. D. Thangadurai, S. Yoon, *Tetrahedron Lett.*, 2011, 52, 2645–2648.
https://doi.org/10.1016/j.tetlet.2011.03.048.
[36] Y. Iimura, T. Sakurai, K. Yamamoto, *Bull. Chem. Soc. Jpn.*, 1988, 61, 821–826.
https://doi.org/10.1246/bcsj.61.821.
[37] D. V. Konarev, S. S. Khasanov, G. Saito, R. N. Lyubovskaya, Y. Yoshida, A. Otsuka, *Chem. Eur. J.*, 2003, 9, 3837–3848.
https://doi.org/10.1002/chem.200204470.
[38] W. R. Scheidt, *J. Am. Chem. Soc.*, 1974, 97, 84-89.
https://pubs.acs.org/doi/pdf/10.1021/ja00808a013.
[39] Z.-S. Li, J.-S. Chai, *Acta Crystallogr. E.*, 2007, 63, m1533–m1535.
https://doi.org/10.1107/S1600536807015061.
[40] M.-C. Suen, Y.-H. Wang, J.-C. Wang, *J. Chin. Chem. Soc.*, 2004, 51, 43–48.
https://doi.org/10.1002/jccs.200400008.

[41] K. Muller-Buschbaum, F. Schonfeld, CSD Communication (Private Communication) (2014), CCDC 1037419, (2014).

[42] J.-H. Yu, Q. Hou, T.-G. Wang, X. Zhang, J.-Q. Xu, *J. Solid State Chem.*, 2007, 180, 518–522. https://doi.org/10.1016/j.jssc.2006.10.028.

[43] Jin-Zhong Gu • Dong-Yu Lv • Zhu-Qing Gao • Jian-Zhao Liu • Wei Dou, *Transit. Met. Chem.* (2011) 36:53–58, DOI 10.1007/s11243-010-9433-3

[44] M. A. Spackman, D. Jayatilaka, *CrystEngComm*, 2009, 11, 19–32. https://doi.org/10.1039/B818330A.

[45 M. A. Spackman, J. J. McKinnon, *CrystEngComm*, 2002, 4, 378–392. https://doi.org/10.1039/B203191B.

[46] M. J. Turner, J. J. McKinnon, S. K. Wolff, D. J. Grimwood, P. R. Spackman, D. Jayatilaka, M. A. Spackman, *CrystalExplorer17*, The University of Western Australia Perth, WA, Australia, 2017.

[47] J. J. McKinnon, D. Jayatilaka, M. A. Spackman, *Chem. Commun.*, 2007, 3814–3816. https://doi.org/10.1039/B704980C.

[48] Book review, *J. Am. Chem. Soc.*, 2002, 124, 1830–1830. https://doi.org/10.1021/ja0153520.

[49] A. Mansour, Y. Belghith, M. S. Belkhiria, A. Bujacz, V. Guérineau, H. Nasri, *J. Porphyr. Phthalocyanines,* 2013, 17, 1094–1103. https://doi.org/10.1142/S1088424613500843.

[50] M. Albrecht, P. Maji, C. Häusl, A. Monney, H. Müller-Bunz, *Inorg. Chim. Acta.*, 2012, 380, 90–95. https://doi.org/10.1016/j.ica.2011.08.039.

[51] H. Sugimoto, N. Ueda, M. Mori, *Bull. Chem. Soc. Jpn.*, 1981, 54, 3425–3432. https://doi.org/10.1246/bcsj.54.3425.

[52] A. Shirazi, H. M. Goff, *Inorg. Chem.*, 1982, 21, 3420-3425. https://pubs.acs.org/doi/pdf/10.1021/ic00139a030.

[53] N. Amiri, S. Nouir, M. Hajji, T. Roisnel, T. Guerfel, G. Simonneaux, H. Nasri, *J. Saudi Chem. Soc.*, 2019, 23, 781–794. https://doi.org/10.1016/j.jscs.2019.03.003.

[54] Y. Belghith, A. Mansour, J.-C. Daran, H. Nasri, *Open J. Inorg. Chem.*, 2012, 2, 81–87. https://doi.org/10.4236/ojic.2012.24012.

[55] J. R. Darwent, P. Douglas, A. Harriman, G. Porter, M.-C. Richoux, *Coord. Chem. Rev.*, 1982, 44, 83–126. https://doi.org/10.1016/S0010-8545(00)80518-4.

[56] C. Paul-Roth, J. Rault-Berthelot, G. Simonneaux, C. Poriel, M. Abdalilah, J. Letessier, *J. Electroanal. Chem.*, 2006, 597, 19–27. https://doi.org/10.1016/j.jelechem.2006.07.039.

[57] K. M. Kadish, M. M. Morrison, *J. Am. Chem. Soc.*, 1976, 98, 3326–3328. https://doi.org/10.1021/ja00427a046.

[58] S. Nasri, I. Zahou, I. Turowska-Tyrk, T. Roisnel, F. Loiseau, E. Saint-Amant, H. Nasri, *Eur. J. Inorg. Chem.*, 2016, 2016, 5004–5019. https://doi.org/10.1002/ejic.201600575.

[59] X. Ke, R. Kumar, M. Sankar, K. M. Kadish, *Inorg Chem*, 2018, 57, 1490–1503. https://doi.org/10.1021/acs.inorgchem.7b02856.

[60] K. M. Kadish, X. H. Mu, X. Q. Lin, *Inorg. Chem. (Print)*, 1988, 27, 1489–1492. https://doi.org/10.1021/ic00281a035

[61] L. A. Truxillo, D. G. Davis, *Anal. Chem.,* 1975, 47, 2260-2267. https://pubs.acs.org/doi/pdf/10.1021/ac60363a052.

[62] J. M. Assour, *J. Chem. Phys.*, 1965, 43, 2477–2489. https://doi.org/10.1063/1.1697147.

[63] F. A. Walker, *J. Am. Chem. Soc.*, 1970, 92, 4235–4244. https://doi.org/10.1021/ja00717a018.

[64] B. B. Wayland, M. E. Abd-Elmageed, *J. Am. Chem. Soc.*, 1974, 96, 4809–4814. https://doi.org/10.1021/ja00822a017.

[65] G. P. Daeges, J. Huettermann, *J. Phys. Chem.,*1992, 96, 4787-4794.

https://pubs.acs.org/doi/pdf/10.1021/j100191a013.

[66] S. Chowdhury, P. Das, *Sep. Sci. Technol*., 2011, 46, 1966–1976. https://doi.org/10.1080/01496395.2011.584930.

[67] P. O. Bedolla, G. Feldbauer, M. Wolloch, S. J. Eder, N. Dörr, P. Mohn, J. Redinger, A. Vernes, *J. Phys. Chem. C*, 2014, 118, 17608−17615. https://doi.org/10.1021/jp503829c

[68] C. Tejada Tovar, Á. Villabona Ortiz, L. E. Garcés Jaraba, *Ing. y Univ.*, 2015, 19, 283–298. https://doi.org/10.1114/javeriana.iyu19-2.kamr.

[69] B. C. Nyamunda, F. Chigondo, *J. Atoms, Mol.*, 2013, 3, 23–44.

[70] C.-H. Liao, S.-F. Kang, F.-A. Wu, *Chemosphere*, 2001, 44, 1193–1200. https://doi.org/10.1016/S0045-6535(00)00278-2.

[71]M. Khairy, E. M. Naguib, M. M. Mohamed, *J. Photochem. Photobio*l. A. 2020, 396, 112507. https://doi.org/10.1016/j.jphotochem.2020.112507.

[72] A. M. Mostafa, E. A. Mwafy, *J. Mol. Struct.*, 2020, 1221, 128872. https://doi.org/10.1016/j.molstruc.2020.128872.

[73] W. Zhang, X. Xiao, T. An, Z. Song, J. Fu, G. Sheng, M. Cui, *J. Chem. Technol. Biotechnol.*, 2003, 78, 788–794.https://doi.org/10.1002/jctb.864.

[74] J. Zia, E. S. Aazam, U. Riaz, *J. Mater. Res. Technol.*, 2020, 9, 9709–9719. https://doi.org/10.1016/j.jmrt.2020.06.048.

[75] S.-Z. Kang, Y.-K. Yang, W. Bu, J. Mu, *J. Solid State Chem.*, 2009, 182, 2972–2976. https://doi.org/10.1016/j.jssc.2009.08.014.

[76] C. Wang, J. Li, G. Mele, G.-M. Yang, F.-X. Zhang, L. Palmisano, G. Vasapollo, *Appl. Catal. B*, 2007, 76, 218–226.https://doi.org/10.1016/j.apcatb.2007.05.028.

[77] W. Sun, J. Li, G. Yao, M. Jiang, F. Zhang, *Catal. Commun.*, 2011, 16, 90–93. https://doi.org/10.1016/j.catcom.2011.09.013.

Synthesis, structural, spectroscopic and electrochemical characterization of two new cobalt(II) piperazine *meso*-arylporphyrins (Complexes **1** and **2**). These two compounds were used as efficient absorbents.

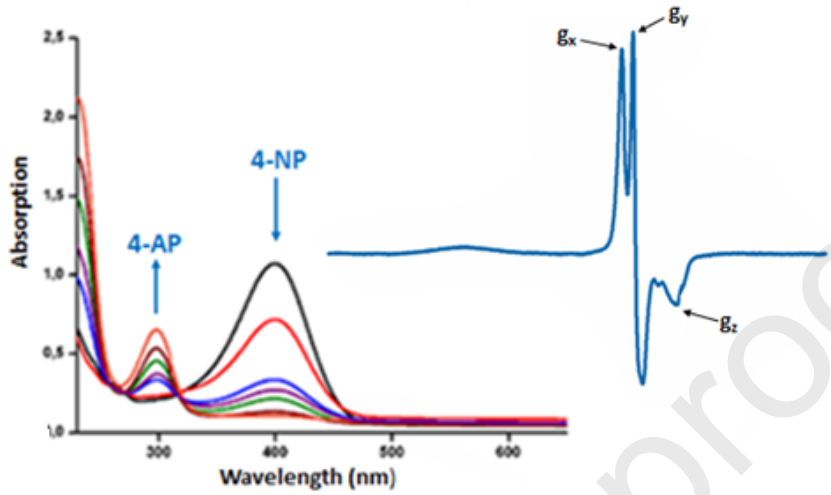

Mouhieddinne Guergueb: Investigation,

Soumaya Nasri: Investigation-Methodology,

Jihed Brahmi: Investigation-Writing,

Youssef O. Al-Ghamdi: Visualization,

Frédérique Loiseau: S*upervi*sion,

Florian Molton: Formal analysis,

Thierry Roisnel: Formal analysis,

Vincent Guerineau: Visualization-Formal analysis,

Habib Nasri: Project administration-Writing - Original Draft.